20. X. Z. Xu, thesis, Université Paris VI (1993).
21. RIBER Instruments SA Group, 133 Bd National, 92503 Rueil Malmaison, France.
22. X. Z. Xu, M. Viret, H. Tebbji, M. Laguës, *Appl. Superconductivity* 1, 755 (1993).
23. We acknowledge G. Deutscher for numerous useful and encouraging discussions during the past 6 years. We also thank N. Bontemps and P. Monod for the magnetization measurements and P. Luzeau for the MBE deposition equipment.

18 November 1993; accepted 22 November 1993

The Transition State of the F + H_2 Reaction

David E. Manolopoulos, Klaus Stark, Hans-Joachim Werner,
Don W. Arnold, Stephen E. Bradforth, Daniel M. Neumark

The transition state region of the F + H_2 reaction has been studied by photoelectron spectroscopy of FH_2^-. New *para* and *normal* FH_2^- photoelectron spectra have been measured in refined experiments and are compared here with exact three-dimensional quantum reactive scattering simulations that use an accurate new ab initio potential energy surface for F + H_2. The detailed agreement that is obtained between this fully ab initio theory and experiment is unprecedented for the F + H_2 reaction and suggests that the transition state region of the F + H_2 potential energy surface has finally been understood quantitatively.

The transition state plays a central role in chemical reaction dynamics (*1*). Asymptotically observable quantities such as integral cross sections and thermal rate constants often depend crucially on what happens in a relatively narrow region around the transition state saddle point, and a number of approximate and exact theories of bimolecular exchange reactions exploit this (*2*). It is therefore particularly interesting if an experiment can be devised to look directly at the transition state, without having to infer what happens there from asymptotic measurements. The photoelectron spectroscopy of stable negative ions such as FH_2^- is one such experiment that has been developed recently at Berkeley (*3*). In favorable circumstances, when the equilibrium geometry of the anion lies close to the neutral transition state, the photoelectron spectrum of the anion can give a direct vibrationally resolved picture of the transition state dynamics and so realize the goal of "transition state spectroscopy."

The circumstances are particularly favorable for FH_2^-, which photodetaches close to the transition state of one of the most thoroughly investigated reactions in chemical dynamics. Various aspects of the (asymptotic) product energy and angular distributions of the F + H_2 reaction have been measured in chemical laser (*4*), infrared chemiluminescence (*5*), and crossed molecular beam experiments (*6*), for example, and accurate thermal rate constants have been obtained over a large temperature range (*7*). The reaction has also played a key role in the development of quantum reactive scattering theory, with its high exoergicity, unsymmetrical mass combination, pronounced resonance structure, and experimental accessibility all making it a prime target for study (*8*). Moreover, the challenges posed by the transition state region of the F + H_2 potential energy surface (PES) have long made it a favorite problem in electronic structure theory (*9*), and numerous global F + H_2 potential energy functions have been proposed (*10, 11*).

Given this background and encouraging early work on the FH_2^- system by Zhang and Miller (*12*) and Weaver and Neumark (*13*), four of the present authors have recently completed a detailed experimental and theoretical study of the FH_2^- photoelectron spectrum (*14*). Experiments were performed in this study for both *para* and *normal* FH_2^-, that is FH_2^- ions prepared by clustering F^- with both *para* and *normal* hydrogen, and three previously proposed semiempirical F + H_2 PESs (*11*) were used in quantum mechanical simulations of the resulting spectra. (Recall that in *para* H_2 only the even rotational levels are populated, whereas in *normal* H_2 the odd:even population ratio is 3:1.) The study succeeded in showing that the *para* and *normal* FH_2^- photoelectron spectra are dominated by bending progressions associated with the F + H_2 transition state region and are therefore highly sensitive to the details of the F + H_2 bending potential in this region. None of the three F + H_2 PESs used in the quantum dynamics simulations was particularly successful, however, in giving a truly quantitative prediction of the experimental spectra (*14*).

The inadequacies of the semiempirical surfaces suggest that a better approach is to construct a fully ab initio PES for F + H_2, which has proved a considerable challenge. The main problem is that both the classical barrier height and the bending potential at the transition state are highly sensitive to electron correlation, and very large orbital and configuration basis sets are required if they are to be converged to chemical accuracy (*9, 15, 16*). However, a recent benchmark full configuration interaction (CI) calculation by Knowles *et al.* (*15*) and systematic studies of the convergence of the topology of the FH_2 transition state with respect to the orbital basis and electron correlation treatment (*16*) have shown that the barrier height and reaction exothermicity can now be obtained to sufficient accuracy for dynamics calculations. Calculations at this level of convergence are highly sophisticated and require the use of very large orbital basis sets, extended internally contracted multireference CI (MRCI) wave functions (*17*) with complete active space self-consistent field (CASSCF) reference functions (*18*), and application of the Davidson correction (*19*) for the effect of higher excitations (MRCI + Q). Nevertheless, because the barrier height and reaction exothermicity are sensitive to very different regions of the PES and yet are obtained with comparable (0.1 kcal/mol) accuracy (*15, 16*), and because the MRCI + Q calculations are efficient enough to be performed at a large number (~600) of other geometries, a globally accurate F + H_2 PES is promised by this same level of theory. Such a highly correlated ab initio PES for F + H_2 has recently been constructed by two of the present authors (*16*), and the remainder of this report provides the first stringent experimental test of this new surface by comparison with the *para* and *normal* FH_2^- photoelectron spectra.

A two-dimensional cut through the transition state region of the new F + H_2 PES as a contour diagram is shown in Fig. 1, with contours of the *para* FH_2^- vibrational ground state wave function superimposed. The anion wave function is calculated in the harmonic normal mode approximation (*12*) and the best available equilibrium geometry ($R_{F-H_2} = 2.075$ Å, $r_{H-H} = 0.770$ Å, and $\gamma = 0°$) and vibrational frequencies ($\omega_1 = 292\ \mathrm{cm}^{-1}$, $\omega_2 = 773\ \mathrm{cm}^{-1}$, and $\omega_3 = 4143\ \mathrm{cm}^{-1}$) from the ab initio calculations of Nichols *et al.* (*20*) are used. The corresponding *ortho* wave function may be obtained by reversing the sign of one of the two lobes and is degenerate with the *para* wave function in Fig. 1 (*14, 16*).

The key features of the *para* and *normal* FH_2^- photoelectron spectra are already implicit in Fig. 1. The first thing to notice is that the anion wave function has a good

D. E. Manolopoulos, Department of Chemistry, University of Nottingham, Nottingham NG7 2RD, United Kingdom.
K. Stark and H.-J. Werner, Fachbereich Chemie, Universität Bielefeld, Postfach 100131, 33501 Bielefeld, Germany.
D. W. Arnold and D. M. Neumark, Department of Chemistry, University of California, Berkeley, CA 94720.
S. E. Bradforth, Department of Chemistry, University of Chicago, Chicago, IL 60637.

Franck-Condon overlap with the neutral transition state, as has already been mentioned above. The FH_2^- equilibrium geometry given by Nichols *et al.* is linear with F–H and H–H distances of 1.690 and 0.770 Å (20), for example, and the corresponding distances at the two degenerate saddle points on the F + H_2 surface are similar at 1.541 and 0.772 Å (15). Indeed, the fact that the H–H bond length changes so little from the anion to the neutral in the Franck-Condon region is what allows us to eliminate this coordinate from Fig. 1 without losing any essential information. The physical implication of the small H–H bond length change is minimal H_2 vibrational excitation on photodetachment (see below).

The second thing to notice about Fig. 1 is that, in contrast to the linear equilibrium geometry of the anion, the saddle points on the new F + H_2 surface are bent at an F–H–H bond angle of 119° (15). The coordinate which experiences the largest change in potential energy on photodetachment is therefore a bending coordinate, which explains why the observed FH_2^- photoelectron spectra are dominated by bending progressions (14). It also explains why the *para* and *normal* FH_2^- photoelectron spectra are so different, with the former only containing transitions to bending states that correlate asymptotically with F + H_2 (even *j*) and the latter containing transitions to states that correlate with both F + H_2 (odd *j*) and F + H_2 (even *j*) in the usual 3:1 *ortho:para* ratio.

According to the model developed by Schatz (21), and adapted for the present problem by Zhang and Miller (12), the FH_2^- photoelectron spectrum can be simulated quantum mechanically through the calculation of a simple Franck-Condon factor:

$$P(E) = \sum_{n} |\langle \Psi_n(E) | \Psi_i \rangle|^2 \qquad (1)$$

Here $\Psi_n(E)$ is an energy-normalized F + H_2 reactive scattering wave function at energy E with asymptotic quantum numbers n, and Ψ_i is the initial rovibrational wave function of the anion. [In practice, the permutation symmetry of the two hydrogens can be exploited to reduce Eq. 1 to two separate Franck-Condon factors, one each for *ortho* and *para*, and these can then be combined in the appropriate ratio to simulate the *normal* FH_2^- spectrum (14).] The use of this model to simulate an anion photoelectron spectrum involves several fundamental assumptions, including in particular the assumption that the transition moment μ_{fi} for the electronic transition is a constant function of both the nuclear coordinates in the Franck-Condon region and the scattering energy E of the neutral photofragments (22). However, the results presented below suggest that these assumptions are justified for FH_2^-.

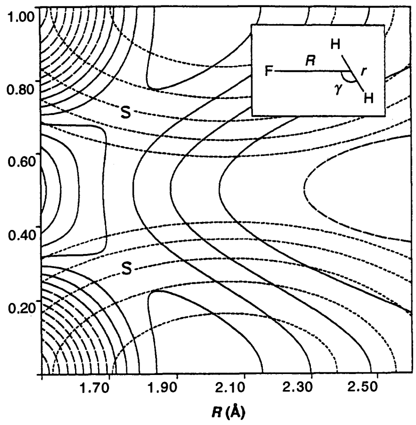

Fig. 1. The transition state region of the F + H_2 PES and its overlap with the FH_2^- anion wave function. The solid lines are contours of the new F + H_2 PES in steps of 0.4 kcal/mol from 0.4 to 2.8 kcal/mol, relative to the bottom of the asymptotic F + H_2 valley. The long dashed lines are similar contours from −2.8 to 0.0 kcal/mol. The short dashed lines are contours of the *para* FH_2^- anion wave function, each successive contour representing a decrease in the square modulus of the wave function by a factor of 10. The coordinates of the plot are the F–H_2 distance *R* and the Jacobi angle γ that are illustrated in the inset; the H–H bond length *r* is fixed at 0.771 Å throughout (see text). The F + H_2 transition state saddle points (S) occur along minimum potential energy paths between a C_{2v} symmetry van der Waals well in the F + H_2 reactant valley and the two degenerate H + HF product valleys.

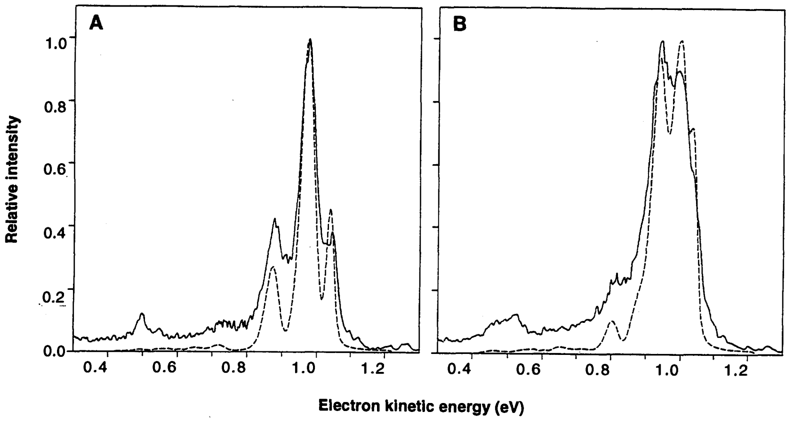

Fig. 2. Comparison between experimental (solid line) and theoretical (dashed line) FH_2^- photoelectron spectra: (**A**) *para* FH_2^- and (**B**) *normal* FH_2^-. The experimental spectra were obtained in refined experiments as described in the text. The theoretical spectra were obtained from Eqs. 1 and 2 by performing exact three-dimensional quantum reactive scattering calculations on the new F + H_2 PES and convoluting the resulting *P*(*E*)s with a Gaussian (19 meV full-width at half-maximum) to approximate the experimental resolution in the neighborhood of the dominant peaks.

Theoretical simulations of the *para* and *normal* FH_2^- photoelectron spectra have been performed on the new F + H_2 surface by using an exact quantum reactive scattering method by Schatz (23) for calculating the reactive scattering wave functions in Eq. 1 in conjunction with the harmonic normal mode approximation for the anion. Full three-dimensional quantum reactive scattering calculations such as these have only become possible quite recently as a result of a revolution in computational methodology (24). However, the present anion photoelectron spectrum simulations are comparatively straightforward because only a few angular momentum states of the (rotationally cold) anion are expected to be populated in the experiment. This means that only a few partial waves of the neutral reaction contribute, and $J = 0$ provides a good approximation to the full spectrum. Therefore, in addition to being particularly sensitive to the transition state region and largely immune to the angular momentum averaging that washes dynamical structure out of more conventional full-collision measurements (25), the FH_2^- photoelectron spectrum provides a probe of the F + H_2 PES that is computationally very accessible.

The present theoretical simulations are shown superimposed on new experimental FH_2^- spectra in Fig. 2. The only parameter in the simulations that is not yet known with any great accuracy is the dissociation energy D_0 of the anion, for which the ab initio calculations of Nichols *et al.* give $D_0 = 0.20 \pm 0.10$ eV (20). This parameter enters the energy conservation relation between the photoelectron kinetic energy *e*KE, the energy of the incident photon (4.657 eV), the electron affinity of fluorine [EA(F), 3.401 eV], the zero point energy (ZPE) of H_2 (0.268 eV), and the scattering energy E relative to the bottom of the asymptotic F + H_2 reactant valley (13, 14):

$$eKE = h\nu - D_0(FH_2^-) - EA(F) + ZPE(H_2) - E \qquad (2)$$

In Fig. 2, D_0 has been adjusted to align the main peaks in the simulated and experimental *para* FH_2^- spectra, giving $D_0 = 0.205$ eV, and the same relation between *e*KE and *E* has been used for *normal* FH_2^-. The theoretical spectra have also been convoluted with a Gaussian (full-width at half-maximum of 19 meV) to approximate the experimental resolution at *e*KE = 1.0 eV.

The new experimental spectra in Fig. 2 were obtained with the same apparatus as described previously (*14*), with photoelectrons collected parallel to the electric field vector of the (plane polarized) photodetachment laser so as to minimize the contribution from excited F + H_2 electronic states (*13*). However, both spectra have been significantly improved. In particular, the contribution from excited F + H_2 electronic states has been further reduced by improving the purity of the laser polarization. The effect of this improved polarization is well illustrated by the region *e*KE < 0.8 eV, where the photoelectron signals are close to baseline in both spectra; this is precisely the region in which transitions to excited F + H_2 electronic states are expected to be most pronounced (*14*).

Another more important modification was also used to obtain the *para* FH_2^- spectrum in Fig. 2A. The experimental *para* FH_2^- spectrum shown in our earlier paper consisted of a broad central feature with some partially resolved features on either side (*14*), whereas considerably more structure was found in the simulations. We postulated there that the experimental spectrum was likely to be contaminated by a certain amount of *para* → *ortho* conversion on the walls of the gas mixing cylinder prior to the experiment, and the evidence for this was made even stronger by the present theoretical calculations. The spectrum shown in Fig. 2A was therefore obtained in a new experiment prior to which the NF_3/*para* H_2 mixture was held in an aluminum (rather than stainless steel) gas cylinder so as to reduce the conversion. The effect of this final modification was found to be quite dramatic, and indeed the experimental *para* FH_2^- spectrum in Fig. 2A shows three pronounced peaks between *e*KEs of 0.8 and 1.1 eV. This improvement allows a considerably more detailed comparison with theory than was possible with the earlier data.

The assignment of the FH_2^- photoelectron spectra in Fig. 2 is similar to that deduced in our earlier paper from simulations on other F + H_2 PESs (*14*). Thus, the two peaks in the *para* FH_2^- spectrum in Fig. 2A at *e*KE = 0.974 and 0.877 eV are transitions to $F/H_2(j)$ bending (or hindered rotor) states with quantum numbers $j = 2$ and 4, in order of decreasing *e*KE (see Eq. 2). A one-dimensional bending simulation (*14*) on the new F + H_2 PES reveals that the $F/H_2(j = 0)$ peak occurs with low intensity just above *e*KE = 1.0 eV, but this peak is not really discernable in either the three-dimensional simulations or the experiment. The three peaks in the *normal* FH_2^- spectrum in Fig. 2B at *e*KE = 0.993, 0.943, and 0.815 eV are transitions to $F/H_2(j)$ hindered rotor states with quantum numbers $j = 1$, 3, and 5. These *ortho* peaks are more apparent than the *para* peaks because of the 3:1 *ortho:para* ratio. The small peaks at *e*KE ≈ 0.5 eV in both spectra are transitions to F/H_2 states that correlate with vibrationally excited $H_2(v = 1)$; the fact that these peaks are not so pronounced in the theoretical simulations suggests that the harmonic normal mode approximation may be somewhat inadequate for the anion, and requires further investigation. Finally, the narrow peak in the *para* FH_2^- spectrum at *e*KE = 1.044 eV is due to a scattering resonance associated with a quasi-bound state in the H + HF product valley. In contrast to the pure bending states of the F + H_2 transition state, which are restricted by symmetry to either *para* or *ortho* FH_2^-, this resonance contribution shows up at the same scattering energy (between *E* = 0.280 and 0.285 eV) in both simulations. It is therefore particularly pleasing that it is also seen in the improved experimental *normal* FH_2^- spectrum as a small bump on the shoulder of the $F/H_2(j = 1)$ peak at *e*KE = 1.035 eV. These assignments are summarized in Table 1.

Table 1. Assignment of peaks in the FH_2^- photoelectron spectra (Fig. 2).

Peak position (eV)	Assignment
	para *FH_2^-*
1.044	H/HF resonance
0.974	$F/H_2(v = 0, j = 2)$
0.877	$F/H_2(v = 0, j = 4)$
~0.5	$F/H_2(v = 1)$
	normal *FH_2^-*
1.035*	H/HF resonance
0.993	$F/H_2(v = 0, j = 1)$
0.943	$F/H_2(v = 0, j = 3)$
0.815	$F/H_2(v = 0, j = 5)$
~0.5	$F/H_2(v = 1)$

*Shoulder.

Although the assignments are similar to those given before, the detailed quantitative agreement between theory and experiment in Fig. 2 is far better than it was possible to obtain previously (*14*). In part, this is because of the improved experimental spectra, which are significantly better resolved than before. However, theoretical simulations were also performed on three widely used semiempirical F + H_2 PESs in our earlier study, and in no case did the results agree in such quantitative detail with the experimental peak positions, widths, and intensities for both *para* and *normal* FH_2^- as those in Fig. 2. Moreover, this improvement in the theoretical spectra is attributable solely to the improved accuracy of the present ab initio F + H_2 surface in the transition state region, because our earlier simulations used the same harmonic normal mode parameters for FH_2^-. Thus, the present combination of ab initio electronic structure theory, ab initio quantum dynamics, and a novel transition state spectroscopy experiment would appear finally to have converged on an accurate description of the F + H_2 transition state region.

It will be interesting in future work to see whether the agreement between theory and experiment in Fig. 2 can be made even better by going beyond the harmonic normal mode approximation to the FH_2^- anion, which is probably the largest single approximation in the present model. It will also be interesting to see whether the present F + H_2 PES gives a good quantitative prediction of the asymptotic experimental properties of the F + H_2 reaction, such as the HF product vibrational branching ratio and angular distributions (*4*–*6*). These properties provide a sensitive probe of the PES in the H + HF product valley and so are somewhat complementary to the transition state spectroscopy measurements considered here.

REFERENCES AND NOTES

1. For example, see *Faraday Discuss. Chem. Soc.* **91**, 1 (1991).
2. W. H. Miller, *Acc. Chem. Res.* **26**, 174 (1993).
3. R. B. Metz, S. E. Bradforth, D. M. Neumark, *Adv. Chem. Phys.* **81**, 1 (1992); D. M. Neumark, *Annu. Rev. Phys. Chem.* **43**, 153 (1992); *Acc. Chem. Res.* **26**, 33 (1993).
4. J. H. Parker and G. C. Pimentel, *J. Chem. Phys.* **51**, 91 (1969); R. D. Coombe and G. C. Pimentel, *ibid.* **59**, 251 (1973); M. J. Berry, *ibid.*, p. 6229.
5. J. C. Polanyi and D. C. Tardy, *J. Chem. Phys.* **51**, 5717 (1969); J. C. Polanyi and K. B. Woodall, *ibid.* **57**, 1574 (1972); N. Jonathan, C. M. Melliar-Smith, D. H. Slater, *Mol. Phys.* **20**, 93 (1971).
6. D. M. Neumark, A. M. Wodtke, G. N. Robinson, C. C. Hayden, Y. T. Lee, *J. Chem. Phys.* **82**, 3045 (1985).
7. E. Wurzburg and P. L. Houston, *ibid.* **72**, 4811 (1980); R. F. Heidner, J. F. Bott, C. Gardner, J. E. Melzer, *ibid.*, p. 4815.
8. G. C. Schatz, J. M. Bowman, A. Kuppermann, *ibid.* **63**, 674 (1975); J. N. L. Connor, W. Jakubetz, J. Manz, *Mol. Phys.* **35**, 1301 (1978); M. J. Redmon and R. E. Wyatt, *Chem. Phys. Lett.* **63**, 209 (1979); C-H. Yu, D. J. Kouri, M. Zhao, D. G. Truhlar, *ibid.* **157**, 491 (1989); Z. Bacic, J. D. Kress, G. A. Parker, R. T. Pack, *J. Chem. Phys.* **92**, 2344 (1990); J. M. Launay and M. LeDourneuf, *Chem. Phys. Lett.* **169**, 473 (1990); J. D. Kress and E. F. Hayes, *J. Chem. Phys.* **97**, 4881 (1992); S. L. Mielke, G. C. Lynch, D. G. Truhlar, D. W. Schwenke, *Chem. Phys. Lett.* **213**, 10 (1993).
9. C. F. Bender, S. V. O'Neil, P. K. Pearson, H. F. Schaefer, *Science* **176**, 1412 (1972); M. J. Frisch, J. S. Binkley, H. F. Schaefer, W. H. Miller, *Chem. Phys. Lett.* **114**, 1 (1985); H. F. Schaefer, *J. Phys. Chem.* **89**, 5336 (1985); R. Steckler, D. W. Schwenke, F. B. Brown, D. G. Truhlar, *Chem. Phys. Lett.* **121**, 475 (1985); D. W. Schwenke, R. Steckler, F. B. Brown, D. G. Truhlar, *J. Chem. Phys.* **84**, 5706 (1986); *ibid.* **86**, 2443 (1987); C.

W. Bauschlicher Jr., S. P. Walch, S. R. Langhoff, P. R. Taylor, R. L. Jaffe, *ibid.* **88**, 1743 (1988); C. W. Bauschlicher Jr., S. R. Langhoff, T. J. Lee, P. R. Taylor, *ibid.* **90**, 4296 (1989).
10. J. T. Muckerman, in *Theoretical Chemistry—Advances and Perspectives*, H. Eyring and D. Henderson, Eds. (Academic Press, New York, 1981), vol. 6A, pp. 1–77.
11. R. Steckler, D. G. Truhlar, B. C. Garrett, *J. Chem. Phys.* **82**, 5499 (1985); T. Takayanagi and S. Sato, *Chem. Phys. Lett.* **144**, 191 (1988); G. C. Lynch, R. Steckler, D. W. Schwenke, A. J. C. Varandas, D. G. Truhlar, *J. Chem. Phys.* **94**, 7136 (1991).
12. J. Z. H. Zhang and W. H. Miller, *J. Chem. Phys.* **92**, 1811 (1990).
13. A. Weaver and D. M. Neumark, *Faraday Discuss. Chem. Soc.* **91**, 5 (1991).
14. S. E. Bradforth, D. W. Arnold, D. M. Neumark, D. E. Manolopoulos, *J. Chem. Phys.* **99**, 6345 (1993).
15. P. J. Knowles, K. Stark, H.-J. Werner, *Chem. Phys. Lett.* **185**, 555 (1991).
16. More details about the ab initio calculations underlying the new F + H_2 surface and the functional form used to represent it will be given in a future publication; K. Stark and H.-J. Werner, unpublished results.
17. H.-J. Werner and P. J. Knowles, *J. Chem. Phys.* **89**, 5803 (1988); P. J. Knowles and H.-J. Werner, *Chem. Phys. Lett.* **145**, 514 (1988).
18. H.-J. Werner and P. J. Knowles, *J. Chem. Phys.* **82**, 5053 (1985); P. J. Knowles and H.-J. Werner, *Chem. Phys. Lett.* **115**, 259 (1985).
19. S. R. Langhoff and E. R. Davidson, *Int. J. Quantum Chem.* **8**, 61 (1974).
20. J. A. Nichols, R. A. Kendall, S. J. Cole, J. Simons, *J. Phys. Chem.* **95**, 1074 (1991).
21. G. C. Schatz, *J. Chem. Phys.* **90**, 3582 (1990); *ibid.*, p. 4847; *J. Phys. Chem.* **94**, 6157 (1990).
22. The final electronic wave function that enters the definition of μ_{fi} is an electron scattering wave function that depends on the electron kinetic energy *e*KE and hence by total energy conservation as in Eq. 2 on the neutral photofragment scattering energy *E*.
23. G. C. Schatz, *Chem. Phys. Lett.* **150**, 92 (1988).
24. D. E. Manolopoulos and D. C. Clary, *Ann. Rep. Prog. Chem. Sect. C* **86**, 95 (1989); W. H. Miller, *Annu. Rev. Phys. Chem.* **41**, 245 (1990); D. G. Truhlar, D. W. Schwenke, D. J. Kouri, *J. Phys. Chem.* **94**, 7346 (1990).
25. G. C. Schatz, *Annu. Rev. Phys. Chem.* **39**, 317 (1988); J. Z. H. Zhang and W. H. Miller, *Chem. Phys. Lett.* **153**, 465 (1988).
26. We thank J. P. Simons and M. Brouard for helpful discussions. Supported by the U.K. Science and Engineering Research Council, the Deutsche Forschungsgemeinschaft (SFB216), the German Fonds der Chemischen Industrie, and the U.S. Air Force Office of Scientific Research (AFOSR-91-0084). D.M.N. is an NSF Presidential Young Investigator and a Camille and Henry Dreyfus Teacher-Scholar.

11 August 1993; accepted 15 October 1993

Nitrogen-15 and Oxygen-18 Characteristics of Nitrous Oxide: A Global Perspective

K.-R. Kim* and H. Craig

The global budget of N_2O shows a significant imbalance between the known rate of destruction in the stratosphere and the estimated rates of natural and anthropogenic production in soils and the ocean. Measurements of the $^{15}N/^{14}N$ and $^{18}O/^{16}O$ ratios in two major tropospheric sources of N_2O, tropical rain forest soils and fertilized soils, show that soil N_2O from a tropical rain forest in Costa Rica and from sugar-cane fields in Maui is strongly depleted in both ^{15}N and ^{18}O relative to mean tropospheric N_2O. A major source of heavy N_2O, enriched in both ^{15}N and ^{18}O, must therefore be present to balance the light N_2O from soils. One such source is the back-mixing flux of N_2O from the stratosphere, which is enriched in ^{15}N and ^{18}O by photolysis and chemistry. However these return fluxes of ^{15}N and ^{18}O are so great that a large oceanic flux of N_2O is required to balance the heavy isotope–enriched stratospheric flux. All these effects will be reflected in climatically related isotopic variations in trapped N_2O in polar ice cores.

Nitrous oxide (N_2O) is an active atmospheric trace gas (tropospheric mixing ratio = 310 ppbv) that is currently increasing in concentration at a rate of ~0.25% per year (*1*). Various sources both natural and anthropogenic have been identified, but the relative importance of these sources has not yet been established, although it seems clear that tropical forest soils are the primary single source (*2, 3*). The atmospheric residence time of N_2O relative to destruction by stratospheric photolysis and chemistry is ~150 years, but known and estimated inputs to the atmosphere are only about half of the flux required to balance the calculated destruction rate (*4*), and reasons for the imbalance are unknown.

Characterization of tropospheric and dissolved oceanic N_2O by the two isotope ratios $^{15}N/^{14}N$ and $^{18}O/^{16}O$ provides important constraints on the geochemistry and sources of this gas (*5*). In this report we extend this approach to a study of N_2O in tropical rain forest soils (*6*) and in stratospheric air. The $^{15}N/^{14}N$ and $^{18}O/^{16}O$ ratios were measured by injecting molecular N_2O directly into the dual-inlet, triple-collecting mass spectrometer SAMSON and simultaneously measuring masses 44, 45, and 46 for the $^{15}N/^{14}N$ and $^{18}O/^{16}O$ isotope ratios (*7*).

Soil-gas samples were collected from natural soils in the rain forest of Costa Rica (*8, 9*) and from fertilizer-treated soils of sugar-cane fields on the island of Maui (*10*). Air samples were withdrawn from existing soil-flux measurement chambers (*11*) and returned to La Jolla where the N_2O-air mixing ratios were determined by ECD gas chromatography, and the isotope ratios were measured. Table 1 shows that quasi-duplicate samples at one Maui site and at one of the Costa Rican sites agree quite well for both the measured N_2O mixing ratios and the end-member isotopic δ values of the soil N_2O (*12*).

Figure 1 shows the soil-N_2O isotopic data and the δ values of tropospheric N_2O (*5*). Although the isotopic values from different soil sites show rather large variations, they are uniformly depleted in the heavy isotopes and isotopically lighter than the tropospheric air and oceanic samples in all cases. On Maui N_2O from the abundant rainfall site is enriched in the heavy isotopes of both N and O relative to N_2O from the dry-side soil. This effect may be due to denitrification in the wet soils, as nitrification in dry soils generally produces isotopically light N_2O (*13, 14*).

These data show that the isotopic ratios of N_2O emitted from soils in both the natural and fertilized states are significantly depleted in ^{15}N and ^{18}O relative to tropospheric N_2O. Thus there must also exist sources of N_2O enriched in the heavy isotopes to balance the input fluxes of light soil-gas N_2O.

One such heavy tropospheric source is the N_2O produced by nitrification in deep ocean water (*5*): these data are also plotted in Fig. 1. The heavy isotope enrichments in these waters increase with depth, but the deep-water production is not a significant tropospheric source. In contrast to these heavy isotope–enriched samples, the δ values of near-surface dissolved N_2O are quite similar to those of tropospheric N_2O but are slightly depleted in ^{15}N and ^{18}O. It is possible that in some oceanic areas of strong regional upwelling such as the Equatorial Eastern Pacific (*15*) and the northwest Indian Ocean (*16*), N_2O brought to the surface may have been produced by denitrification (*17*) and that N_2O produced in this way may be enriched in ^{15}N (*18*), and perhaps in ^{18}O, relative to values for tropospheric air. However the δ values of dissolved N_2O in shallow depths (surface to depths of ~800 m) are quite similar to those of tropospheric N_2O [(*5*), Fig. 1], so that there is a strong buffering effect of subsurface N_2O

Isotope Laboratory, Scripps Institution of Oceanography, University of California at San Diego, La Jolla, California 92093-0220.

*Also: Department of Oceanography, Seoul National University, Seoul, 151-742, Korea.